INTERNATIONAL JOURNAL OF HYDROGEN ENERGY 46 (2021) 38972–38982

Available online at www.sciencedirect.com

ScienceDirect

journal homepage: www.elsevier.com/locate/he

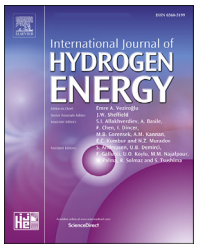

PEM water electrolysis cells with catalyst coating by atomic layer deposition

A. Laube [a,b,*], A. Hofer [c], S. Ressel [a], A. Chica [b], J. Bachmann [c,d], T. Struckmann [a]

[a] Hamburg University of Applied Sciences, Department of Mechanical Engineering and Production Management, Berliner Tor 21, 20099, Hamburg, Germany

[b] Instituto de Tecnología Química, Universitat Politecnica de Valencia-Consejo Superior de Investigaciones Científicas, Avenida de los Naranjos s/n, 46022, Valencia, Spain

[c] Friedrich-Alexander University of Erlangen-Nuernberg, Department of Chemistry and Pharmacy, Chemistry of Thin Film Materials, IZNF/Cauerstr. 3, 91058, Erlangen, Germany

[d] Saint-Petersburg State University, Institute of Chemistry, Universitetskii pr. 26, 198504, St. Petersburg, Russia

HIGHLIGHTS

- Demonstration of a cell design with porous transport electrodes and atomic layer deposition.
- Reduction of catalyst at high mass activity.
- Experimental characterization combined with a detailed overpotential analysis from polarization curve fits

ARTICLE INFO

Article history:
Received 22 June 2021
Received in revised form
15 September 2021
Accepted 18 September 2021
Available online 13 October 2021

Keywords:
PEM water electrolysis
ALD catalyst coating
Porous transport electrodes

ABSTRACT

The limited annual mining capacity and high costs of platinum metal group catalysts (PMG) are confining the production of hydrogen from PEM electrolysis. Therefore, a significant reduction of catalyst needs is crucial to reduce system costs and increase production capacity. This study demonstrates the feasibility of a PEM water electrolysis cell design using porous transport electrodes (PTE) with catalyst coating by atomic layer deposition (ALD) and operation in 1 mol/L sulphuric acid at 60 °C. Though the catalyst loading has been reduced to 0.12 mg/cm^2 iridium on the anode and 0.28 mg/cm^2 platinum on the cathode, a current density of 168 mA/cm^2 and mean high mass activity of 1400 A/g iridium could be achieved at 1.7 V. The characterization of three high loading PTE cells is combined with a detailed overpotential analysis from polarization curve fits and demonstrates a reproducible cell setup. Further analysis steps show an increasing cell performance with increasing coating cycle numbers and the consistency of the anode performance in the three electrode setup with the complete cell. The ALD coated PTE design turns out to be a promising candidate for catalyst loading reduction in PEM electrolysis.

* *Corresponding author*. Hamburg University of Applied Sciences, Department of Mechanical Engineering and Production Management, Berliner Tor 21, 20099, Hamburg, Germany.
E-mail address: armin.laube@haw-hamburg.de (A. Laube).

https://doi.org/10.1016/j.ijhydene.2021.09.153

Introduction

To increase the amount of energy produced from renewable resources, the use of mechanical and electrochemical storage systems are crucial to stabilize electric grids. In the current state, batteries are the most popular electrochemical storage systems. However, water electrolysis is a promising technology to store huge amounts of energy by generating hydrogen which can be converted back to electric energy or used directly in the chemical industry. Alkaline electrolysis is an established and widely used technology to produce hydrogen from electric energy but has the disadvantage of high overpotential and a slow dynamic response. The polymer electrolyte membrane (PEM) electrolysis is now in the focus of research and industry due to a reduced overpotential and a fast response to dynamic power changes. Since PEM electrolyzers are still cost intensive and exhibit limited turn-around due to the need for noble materials and high assembly costs [1], new cell and catalyst concepts are investigated at present. Another reason for the investigation of lower noble catalyst loadings is the limited mining capacity [2–4].

Research on lower catalysts loadings concentrates on catalyst ink composition, membrane coating techniques, the catalyst material and support particles as well as the catalyst application methods to the support particles [5]. Currently PMG catalysts amounts of 2–3 mg/cm^2 are used in commercial PEM electrolysis cells. In the cathode half cell 0.5–1 mg/cm^2 platinum and on the anode half cell 1.5–2.5 mg/cm^2 iridium or ruthenium (oxides) are common [5–8]. The improvement attempts are mainly focused on the anode side due to the slower oxygen evolution reaction (OER) compared to the hydrogen evolution reaction (HER)and due to higher costs for the widely used iridium.

In the past years, several studies with the focus on reduced amounts of iridium catalysts were published. Hegge et al. have achieved a cell performance similar to commercial PEM electrolysis cells with a reduced anode loading of 0.2 mg/cm^2 by combining iridium particles and iridium nano fibers [4].H.Yu et al. were able to reduce the anode catalyst amount to 0.1 mg/cm^2 without performance gains compared to commercial cells by preparing the catalyst powder with reactive spray deposition technology [9,10]. Another approach is the direct coating of the membrane by magnetron sputtering of the membrane, either on a support sublayer [11] or directly on the membrane surface. as shown by T. Hrbek et al. [12]. While the coating technique in commercial applications is the catalyst coating of the membrane (CCM), a promising approach is the use of PTEs with catalyst being coated on the porous transport layer. For the PTE approach, Bühler et al. have shown a comparable cell performance for low current densities and an improved performance for higher current densities with respect to CCM cells [13,14]. An advantage of the PTE design is the suitability to continuous production which is relevant to reduce production costs by large volume productions [15].

ALD as a coating method for catalysts was investigated in solide oxide fuel cells by X.Jiang et al. [16] and was identified as a possible coating method to reduce the catalyst amount in several energy conversion systems by J.Bachmann and Peng [17,18]. Lee et al. applied ALD for the coating of carbon particles with platinum at catalyst coated membranes for PEM fuel cells. They have reported an increased performance compared to commercial carbon supported catalysts, while keeping the amount of platinum constant [19]. Though ALD as a catalyst coating method is currently still a laboratory application, first industrialized applications have been investigated and reported to be a suitable alternative serial production coating process [20,21]. Schlicht et al. developed PTEs by using the ALD method in combination with a previous anodization of titanium felts to coat the OER electrodes with iridium and demonstrated their applicability in reversible fuel cells [22–24] while Ressel et al. have investigated these electrodes in vanadium/air redox flow battery cells [25]. Latest studies on the PTEs with ALD used for catalyst coating were focused on the anodization process parameters of titanium felts to create a nano structured surface which increases the performance and improves the stability of the electrodes [26]. In spite of these efforts, ALD catalyst coated PTEs for PEM electrolysis have only been studied in the 3-electrode half cell laboratory setup and complete cell characterizations are needed.

The ALD PTE cell design is similar to the cell design of commercial CCM PEM electrolysis cells using a PFSA membrane to separate the electrodes. In commercial CCM PEM electrolysis cells the catalyst is applied to the membrane and electrically contacted by conductive porous transport layers. In contrast to that, the PTE cell architecture directly applies the catalyst to the porous transport layers, forming the porous transport electrode as shown in (Fig. 1). By this way

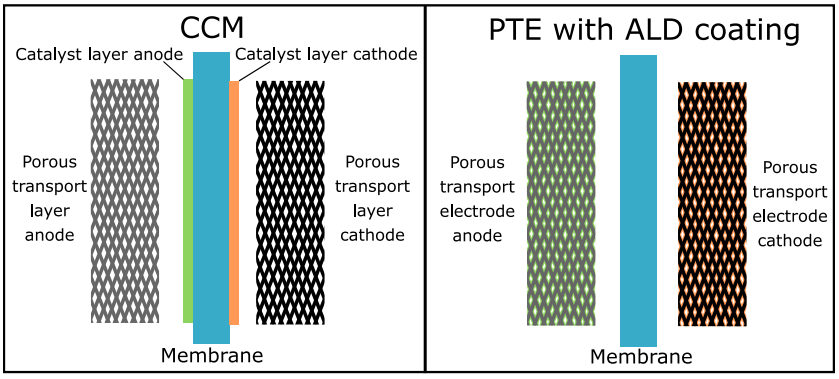

Fig. 1 – Cell architectures in this study - CCM (left) and ALD coated PTEs (right).

the whole surface of the porous layer, including the nano structured surface achieved by the anodization, is catalyst coated and at least in principle, the active area of the electrode is increased.

In the CCM cell setup, the supported catalysts are applied in a mixture with an ion conductive ionomer solution. This layer typically has a thickness of a few microns [5] and thereby a short ionic conduction length. For the ALD PTE setup, the conduction length of the protons is increased up to the thickness of the PTE. To keep the cell's ohmic resistance low, a proper ionomer coating of the PTE will be crucial. In order to allow the investigation of the ALD catalyst coating method prior to optimizing the ionomer coating process in the PTE, the cell can be operated sulphuric acid in both half cells to achieve a sufficiently high protonic conductivity for the whole catalyst coated area.

The aim of this study is to demonstrate the feasibility of ALD catalyst coated PTE cells. The electrochemical characterization is performed in the complete PEM electrolysis cell setup and compared to a standard CCM cell. For the reasons described above the PTE cell is operated in 1 mol/L sulphuric acid. PTEs are produced with two different catalyst loadings to quantify the influence of the ALD thickness. To furthermore verify the reproducibility of the PTE cell architecture, the performances of three individual PTEs with equal catalyst loadings are compared. Polarization curve fits are performed for an overpotential analysis. Finally the operation of the PTE cell in water is evaluated.

Materials

PTE cells with ALD coating

PTE cell anode

Titanium felts from Baekert (ST/Ti/20/350/50)with a thickness of 160 μm a fibre diameter of 20 μm and a porosity of 50% are used for the porous transport electrodes on the anode side. Prior to the ALD coating the titanium felts were anodized following the procedure described in Ref. [26] to create a structure of nanotubes on the whole surface of the titanium felt and thereby increase the electrode surface. Two different catalyst loadings were tested as the iridium catalyst was coated by ALD with 150 cycles and 75 cycles respectively. With respect to the active membrane area, the corresponding catalyst densities are about 0.12 mg/cm^2 and 0.09 mg/cm^2 and were determined by ICP-MS measurements.

PTE cell cathode

On the cathode side an ALD coated graphite felt (SGL Carbon research sample) with a fixed platinum loading is used as porous transport electrodes on the cathode side for all PTE cells. Prior to the ALD coating, the graphite felts were pretreated by thermal activation. The catalyst density is about 0.28 mg/cm^2 platinum as determined by ICP-MS measurements.

PTE preparation and catalyst thin film deposition

Standard chemicals (glycerol and ammonium fluoride) from Carl Roth are used without further purification. For the catalysts methylcyclopentadienyl-iridium(I)- 1,3-cyclohexadiene ((EtCp)Ir(CHD)) and trimethyl (methylcyclopenta-dienyl) platinum (MeCpPtMe3) from Carl Roth are used.

The anode preparation broadly follows the procedure described in Ref. [26]. The titanium felts were anodized using a glycerol electrolyte with 0.5 *wt% NH_4F* and 12 *vol% H_2O* under an applied potential of 40 V for a duration of 4 h in a two-electrode setup with a graphite counter electrode. After rinsing the Ti felts with ethanol and water, the electrodes were soaked in ethanol overnight and dried afterwards. The cathode graphite felts were thermally activated at 450 °C in a muffle furnace from Nabertherm for 3 h in air.

The Ir film was deposited on the anodized titanium felts subsequently using ALD in a commercial Gemstar-6 ALD reactor from Arradiance. (EtCp)Ir(CHD) heated to 90 °C and ozone, generated by an ozone generator model BMT 803 N, were used as precursors, whereas the reaction chamber was maintained at 220 °C. The nominal Ir thickness of 12.5 nm and 5 nm (150 and 75 cycles) was determined on Si wafers by spectroscopic ellipsometry with a SENPro from SENTECH. The scanning electron micrograph (SEM) image in Fig. 2 show the titanium felt before and after anodization and iridium coating by ALD with 150 cycles which indicates a homogeneous coating of the fibre surface. However, energy dispersive X-ray (EDX) measurements on 12 different points over the 5 cm^2 PTE

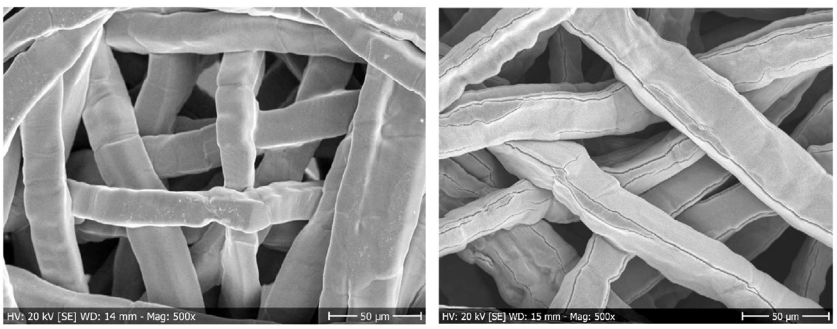

(a) (b)

Fig. 2 – Scanning electron micrographs of titanium felts (a) before and (b) after anodization and iridium catalyst coating with ALD with 150 cycles.

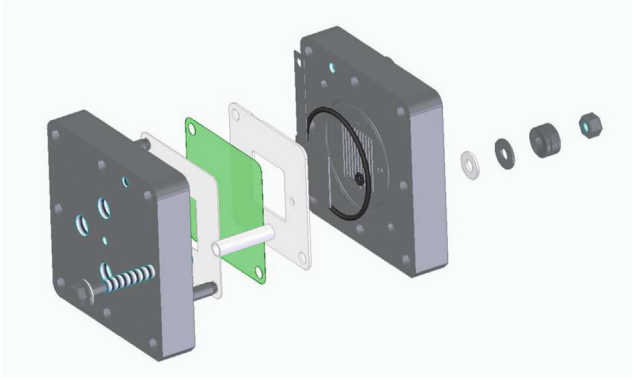

Fig. 3 – Design and assembly of the test cell housing with straight flow fields.

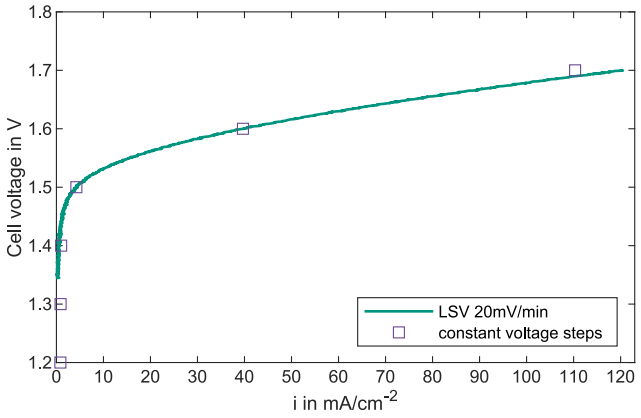

Fig. 4 – Polarization curve recorded with linear sweep voltammetry (green curve) and constant voltage steps (squares). (For interpretation of the references to colour in this figure legend, the reader is referred to the Web version of this article.)

surface indicate an inhomogeneous iridium distribution with a relative standard error of 42% for the mean iridium signal.

The platinum catalyst was applied in a comparable ALD process as for the iridium: (MeCp)PtMe3 heated to 50 °C and ozone were used as precursors (reaction temperature of 220 °C) and Pt was deposited in 30 cycles on the activated graphite felts. This corresponds to a nominal thickness on Si wafers of approx. 2 nm.

Membrane

In the ALD coated PTE cell architecture a fumasep-F10100 membrane (Fumatech BWT) is used without further adjustments.

CCM cell as reference MEA setup

For the gas/liquid diffusion layer of the CCM half cells, titanium and graphite felts identical to the PTE felts are used. The CCM used as a reference for the PTE cell architecture is a Nafion 115 membrane coated with 3 mg/cm^2 Pt/B on the cathode and 3 mg/cm^2 IrRuOx on the anode (FuelCellsETC). The CCM cell is operated with water as common in commercial applications. CCM and PTE cell details are summarized in Table 1. The Nafion 115 membrane of the CCM cell has a thickness 127 μm and a conductivity of 100 *mS/cm* while the F10100 membrane of the PTE cell has a thickness 100 μm and a conductivity of 95 *mS/cm*, which leads to comparable overpotentials caused by the membrane.

Test cell housing

The test cell housing is designed in house and has an active area of 5 cm^2. The two end plates made of titanium grade 2 include the electrolyte feeding, the flow fields, threads for the electric connection and holes for temperature sensors directly behind the flow field. The flow field is made of straight vertical channels with 1.1 mm width and 1 mm depth. The shoulders in between are 0.9 mm wide. On the end plates, sealing frames made of PTFE and expanded PTFE are placed to seal the half cells. The frames are fixed by ceramic pins and thereby keep the electrodes in position. The membrane has the same size as the sealing frames. To reach a good electric connection, the whole setup (cathode, membrane, anode) is compressed by 40% as defined by ceramic and stainless steel spacers (see Fig. 3).

Methods

A scanning electron microscope JEOL JSM 6400 equipped with a LaB6 cathode and an energy dispersive X-ray detector from SAMx was used to investigate the surface of the PTE.

For the electrochemical characterization a potentiostat SP150 in combination with a VMP3 Booster from Biologic was used. The electrolyte/water flow was set to 10 ml/min with a peristaltic pump (Masterflex). All characterizations are performed at 60 °C by using heat plates (CAT-m2021) and temperature sensors in the tanks, fluid cycles and the test cell housing.

The test routine consisted of a membrane break in phase, a heat up phase and the electrochemical characterization. During the membrane break in, a voltage of 1.6 V was applied for 2 h. The heat up took 2 h, while the temperature was nearly constant after 1 h. The techniques used for the electrochemical characterization were polarization curves (PC), electrochemical impedance spectroscopy (EIS), current interrupt (CI) and chronoamperometry (CA) measurements. The PCs were recorded by

Table 1 – Cell components, catalyst coating method and operating media in this study.

Cell ID	Catalyst anode	Catalyst cathode	Membrane	Operating medium
ALD low	Ir 75 cycles	Pt 30 cycles	F10100	1 mol/l H_2SO_4
ALD high,1-3	Ir 150 cycles	Pt 30 cycles	F10100	1 mol/l H_2SO_4
CCM	IrRuOx	Pt/B	Nafion 115	deionised water

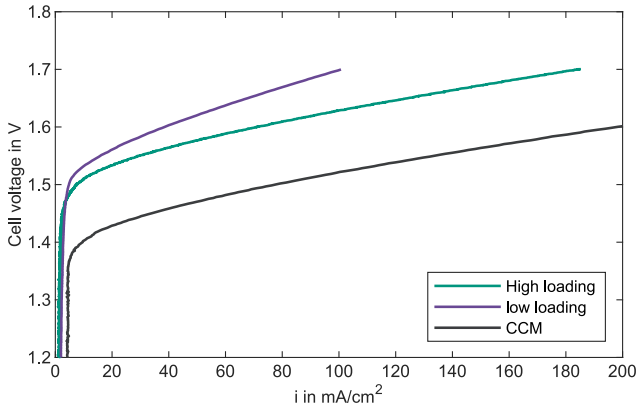

Fig. 5 – Polarization curves of PTE and CCM cells - high loading (green), low loading (purple) and CCM (black). (For interpretation of the references to colour in this figure legend, the reader is referred to the Web version of this article.)

a linear voltage sweep with slope 20 mV/min from 1.2 V to 1.7 V. EIS and CI measurements were performed to investigate the area specific cell resistance (ASR). Two sets of EIS measurements were done as staircase EIS in galvanostatic operation: The first with current densities of 10 mA/cm^2, 15 mA/cm^2 and 20 mA/cm^2 with a 1.5 mA/cm^2 amplitude and a second one with current densities of 25 mA/cm^2, 50 mA/cm^2 and 75 mA/cm^2 with a 1, 5 mA/cm^2 amplitude. Both measurements were done from 100 kHz to 100 mHz with 6 points per decade and 30 s constant current period before each measurement, ASR values were determined as the intercept of the Nyquist plot with the real axis. The standard deviation of the ASR determined with EIS at the different applied current densities is 0.6% for one single cell. The CI measurements were done with three repetitions using applied currents of 10 mA/cm^2, 15 mA/cm^2 and 50 mA/cm^2 which were held for 0.5 s with a relaxing time of 5 s in between and a sampling rate was 2, 500 Hz. The standard deviation of the ASR determined with CI for one single cell over the different applied current densities is 8% respectively 6% for one current density with 6 repetitions. We thus conclude that ASR measurements are sufficiently reproduceable. For the CA measurements, constant voltage was applied in 0.1 V steps from 1.2 V to 1.7 V, holding each step for 2 h. At each voltage step, the mean value of the current over the last hour was determined for validating the PC data recorded with LVS. The cell voltage of all characterization methods was limited to 1.7 V in order to avoid degradation effects during characterizations.

Table 2 – Current densities and ASR of the cell architectures.

Cell	i @ 1,7 V [mA/cm^2]	i @ 1,7 V [A/g]	ASR (EIS) [Ohm × cm^2]	ASR (CI) [Ohm × cm^2]
ALD high loading	185	1540	0.21	0.56
ALD low loading	88	980	0.22	0.77
CCM	326	108	0.47	0.56

Calculation

For investigating the current exchange densities and the ohmic overpotentials of the ALD PTEs an analytical model is fitted to the recorded polarization curves. The model describes the cell voltage as a function of the current density. As described in Ref. [27], the total cell voltage is described by four contributions: the Nernst voltage (E_N), the activation overpotential ($\eta_{Act,Tafel}$), the ohmic overpotential (η_{Ohm}) and the concentration overpotential (η_{Conc}).

$$U(i) = E_N + \eta_{Act} + \eta_{Ohm} + \eta_{Conc} \quad (1)$$

At low current densities, the concentration overpotentials have a minor effect and can be neglected. The description of the cell voltage is then reduced to:

$$U(i) = E_N + \eta_{Act} + \eta_{Ohm} \quad (2)$$

The Nernst voltage at ambient pressure describes the theoretical minimum voltage of the electrolysis cells in this study [28].

$$E_N(T) = 1,229 - 8,5 \times 10^{-4} \times (T - 298) \quad (3)$$

resulting in $E_N = 1.20$ V for an operation temperature T = 60 °C. The activation overpotentials are described by the Tafel equation

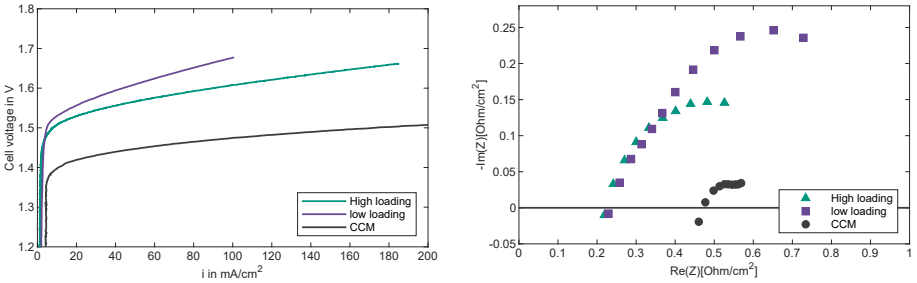

(a) (b)

Fig. 6 – (a) IR-free polarization curves and (b) Nyquist EIS plot for the cell setups - high loading (green), low loading (purple) and CCM (black). (For interpretation of the references to colour in this figure legend, the reader is referred to the Web version of this article.)

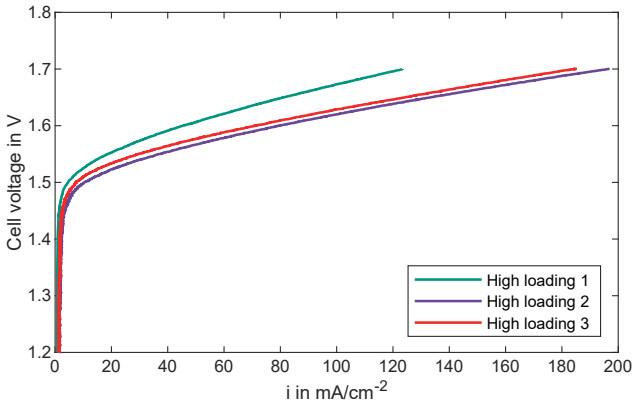

Fig. 7 – Polarization curves of high ALD loading PTE cells.

$$\eta_{Act} = b.ln(\frac{|i|}{i_0}) \quad (4)$$

with exchange current density i_0. The Tafel slope b is given by

$$b = \frac{RT}{\alpha zF} \quad (5)$$

with the ideal gas constant R, the Faraday constant F and the charge transfer coefficient α. The ohmic overpotential arise from the internal area specific cell resistance ASR or R_i:

$$\eta_{Ohm} = i \times R_i \quad (6)$$

Results and discussion

Feasibility and performance of the ALD coated PTE setup

Prior to comparing the performances of electrolysis cells we validate the polarization curve measurements with CA data. Fig. 4 shows the current densities of a high loading PTE cell for cell voltages from 1.2 V to 1.7 V. The polarization curve was recorded with LVS (scan rate 20 mV/min) after 12 *h* stepwise CA measurement with 2 *h* holding time for each step. The CA current density values are determined by the mean value over the last hour of each step. It turns out that for cell voltages up to 1.6 V the current densities are almost identical, just the last current density at 1.7 V shows a slightly higher value for the CA measurement. The polarization curve measurement with LVS at 20 mV/min is thus considered as a validated method and will be used in the following discussion.

We compare cell performances by analysing polarization curves at 60 °C and ambient pressure which were taken after the membrane break in and heat up phases. The polarization curves of one high loading PTE cell, the low loading PTE cell and the CCM reference cell are displayed in Fig. 5. At 1.7 V the high loading PTE cell exhibits a maximum current density of 185 mA/cm^2 while the CCM cell exhibits 326 mA/cm^2. Since the PTE cell current densities are well below the CCM values but accompanied by lower catalyst loadings, we consider the corresponding mass activities as current to catalyst mass ratios. The PTE cell exhibit very high mass activities of 1540 A/g (high loading) and 980 A/g (low loading) compared to the CCM cell value of only 108 A/g. We conclude that the feasibility of the ALD approach in the complete cell setup is demonstrated showing very promising mass activities.

The high loading PTE and CCM curve shapes are almost identical but shifted by approximately + 0.1 V for the PTE cell even at very low current densities indicating higher activation overpotentials for this cell setup. In order to exclude the effects of ohmic resistances on the cell performances, Fig. 6a shows the IR-free polarization curves of the cells. IR-correction was performed by subtracting the ohmic overpotential (eq. (6)) using area specific resistances R_i from galvanostatic EIS measurements (100 kHz–1 kHz at 100 mA/cm^2 with 10 mA/cm^2 amplitude at the same operation conditions).

The IR-free polarization curves are qualitatively similar to the complete polarization curves though the overpotential difference of the CCM and PTE cells slightly increases with the current density.

Since different IR-free polarization curve slopes might arise from different ASR measurement methods we determine ASR_{EIS}, taken as the high frequency real axis intersections of the Nyquist plot (Fig. 6b) and ASR_{CI} from current interrupt measurements and displayed in Table 2. The ASR_{EIS} values are $0.21 Ohm \cdot cm^2$ for the high loading PTE cell and $0.47 Ohm \cdot cm^2$ for the CCM cell while the ASR_{CI} is $0.56 Ohm \cdot cm^2$ for both cell set ups. ASR_{EIS} ans ASR_{CI} values could be reproduced with different measurement parameters. Cooper et al. discovered that the CI measurement technique is effected by potential gradients in the electrode which increase with the thickness of the electrode and nonuniform catalyst distribution [29]. By

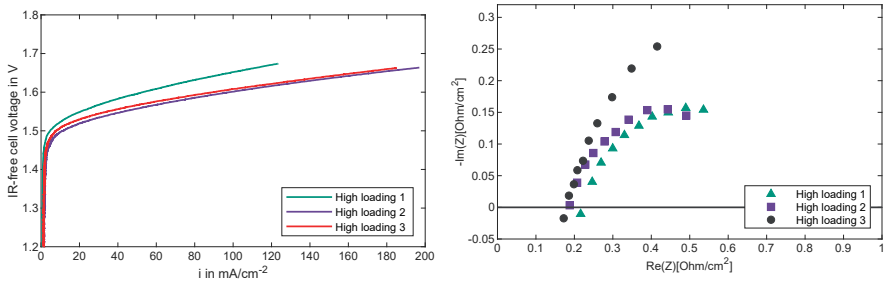

(a) (b)

Fig. 8 – High loading PTE cells: (a) IR-free polarization curves, IR-correction with ASR_{EIS} data, (b) Nyquist plots for ASR_{EIS} determination.

Table 3 – Performance parameters of ALD high loading cells.

Cell	i @ 1,7 V [mA/cm^2]	i @ 1,7 V [A/g]	ASR (EIS) [Ohm × cm^2]	ASR (CI) [Ohm × cm^2]
ALD high 1	123	1025	0.22	0.59
ALD high 2	197	1640	0.19	0.56
ALD high 3	185	1540	0.21	0.30
Mean (std. error)	168 (23)	1400 (200)	0.21 (0.01)	0.48 (0.09)

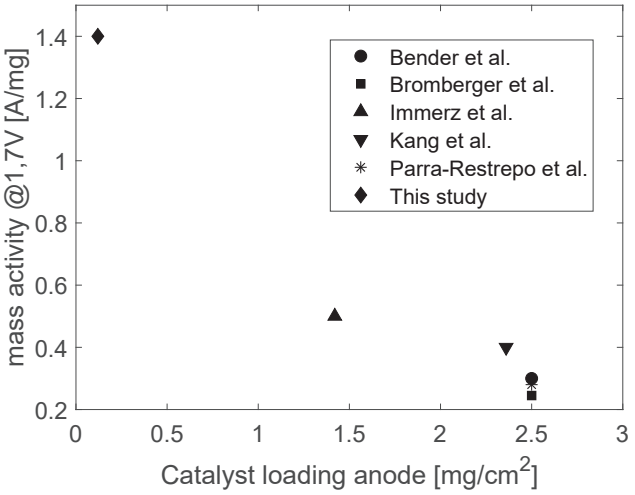

Fig. 9 – Mass activities of ALD catalyst coated PTEs with high loading and data of previous reports (60 °C and ambient pressure).

this way, the difference between the ASR_{EIS} and the ASR_{CI} values for the PTE cell may result from the higher thickness of the catalyst layer covering the whole the porous layer or a nonuniform catalyst layer. The higher ASR_{EIS} value for the CCM cell can be attributed to an additional contact resistance between the PTL and the catalyst layer, while for the PTE cell, the catalyst is coated directly on the conducting porous layer, resulting in a lower contact resistance as observed by Bühler et al. [13].

Amount of catalyst loading

To investigate the influence of the iridium loadings on the cell characteristics.

We compare the polarization curves of the PTE cells with different ALD loading in Fig. 5. Even at low current densities, the cell voltage of the low loading cell exhibits is higher and the difference increases with higher current densities. At the maximum voltage 1.7 V the current density of the lower loading cell is 88 mA/cm^2 and thus roughly half of the higher loading value 168 mA/cm^2. The corresponding mass activity of the low loading is 980 A/g and thus lower than the high loading value 1540 A/g.

The ASR_{EIS} of $0.22 Ohm \cdot cm^2$ (high loading) and $0.21 Ohm \cdot cm^2$ (low) are almost identical (see Table 2) as expected for the identical geometrical architecture and materials. This leads to IR-free cell voltages in Fig. 6a which show no significant changes in the voltage differences of the different loadings.

Table 4 – Reference literature, in parentheses: specific catalyst loadings in *mg/cm^2*.

Author [reference]	Anode Catalyst	Cathode Catalyst
C. Immerz et al. [31]	IrO_2(1.42)	Pt/C (1)
Z. Kang et al. [32]	IrO_2(2.36)	Pt/C (0.78)
G.Bender et al. [30]	Ir (2.5)	Pt (0.8)
K. Bromberger et al. [33]	Ir (2.5)	Pt (0.8)
J.Parra-Restrepo et al. [34]	Ir (2.5)	Pt (0.8)

Reproducibility of the ALD coated PTE cell setup

Three PTE cells high ALD loading cells were identically assembled and characterized in order to investigate the reproducibility of the setup. Their polarization curves, recorded under identical conditions as described above, are shown in Fig. 7, the IR corrected curves are displayed in Fig. 8a. While the performance of two cells is almost identical, the third cell exhibits higher cell voltages, which are still well below the corresponding lower loading values. We summarize the key performance parameters maximum current densities, mass activities and ohmic resistances in Table 3.

The mean value of the current density at 1.7V is 168 mA/cm^2 and exhibits a 14% standard error, mainly due to the third cell, which is still achieving roughly two thirds of the other cell values. ASR_{EIS} values and the real axis intersection frequencies (≈3 kHz) of the Nyquist plots in Fig. 8b are very close to each other. The mean ASR value is close the typical ASR of commercial PEM electrolysis cells [4,5,30], again indicating that no artefacts arise from the ALD PTE approach. As explained above, the ASR_{CI} differences can be attributed to inhomogeneous ALD coating which corresponds to the EDX measurement results of the PTE with high loading.

In Fig. 9 the mass activity of the ALD catalyst coated PTE PEM cell is compared to literature data. The PTE cell values is three to four times higher than the literature values with catalyst loading given in detail in Table 4. The amount of catalyst needed can thus be significantly reduced with the ALD catalyst coated PTE architecture.

In total, we conclude that the general cell setup ist sufficiently well reproducible and achieves promising mass activities.

Cell voltage analysis

In order to analyze the ohmic and activation overpotential contributions to the total cell voltage of the PTE cells, the polarization curve (eq. (2)) is fitted to the experimental data. Fig. 10a displays the whole polarization curve of the high loading PTE cell #3 and the selected part for the fit. For all cells the polarization curves are fitted between 1.45 V and 1.55 V, since in this voltage region, the influence of the concentration overpotential is very low and the fitted transfer coefficients are close to the literature value $\alpha \cdot z = 1$ [35]. The polarization curves of the analyzed cells exhibit parasitic leakage or loss currents of 0.6–0.8 mA/cm^2 at the theoretical Nernst voltage 1.2 V. Since these loss currents are not included in the model, the current densities are shifted by these values before fitting.

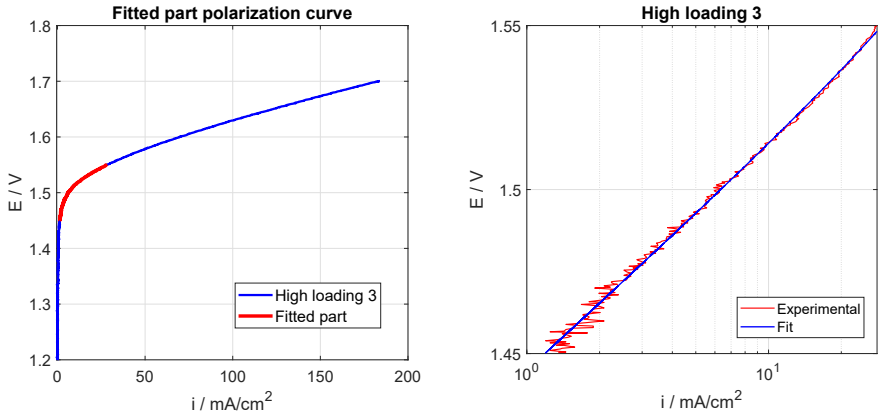

Fig. 10 – High loading PTE #3: (a) polarization curve and fit range (b) experimental and fitted data.

Table 5 – Fit results - activation and ohmic overpotential parameters.

Cell	ASR $[Ohmcm^2]$	i0 $[mA/cm^2]$	α
ALD high 1	0.88	$2 \cdot 10^{-4}$	1.00
ALD high 2	0.62	$3 \cdot 10^{-4}$	1.00
ALD high 3	0.60	$2 \cdot 10^{-4}$	1.01
ALD low	1.06	$1 \cdot 10^{-4}$	0.99
CCM	0.58	$9 \cdot 10^{-3}$	1.00

The leakage currents are expected to result from parasitic reactions like corrosion due to the highly corrosive environment of 1 mol/l sulphuric acid.

Experimental and fitted data ar shown in the Tafel plot of Fig. 10b. While the overall error of the measured and fitted voltage is below 0.002 V for all analyzed cells, the experimental data spread around the fitted data at very low current densities, reflecting the resolution of the measurement equipment.

Fit parameter results are summarized in Table 5. For all PTE cells the fitted *ASR* values are higher than the EIS and CI values whereas the CCM cell *ASR* are close to each other. As explained above, we attribute this difference, which is smaller for the CI values, to the relatively high ionic resistance related to the spatial extension of the PTEs. In addition, linear low current density contributions from concentration overpotentials are assumed to be reflected in ASR_{PC}. Current exchange densities with respect to the membrane cross section of all analyzed cells are between $9 \cdot 10^{-3}\ mA/cm^2$ and $3 \cdot 10^{-4}\ mA/cm^2$ in agreement with values of previously published polarization curve fits [27]. For the ALD coated PTEs the current exchange densities are lower than for the CCM, leading to the observed higher activation overpotentials (eq. (4)).

Up to this study, ALD catalyst coating has not been examined in a complete cell setup, but only in a three electrode setup examining the performance of only one ALD electrode half cell. Since three electrode experiments are much easier to perform and should be used for a first performance measurement, we check for their consistency with the complete cell performance.

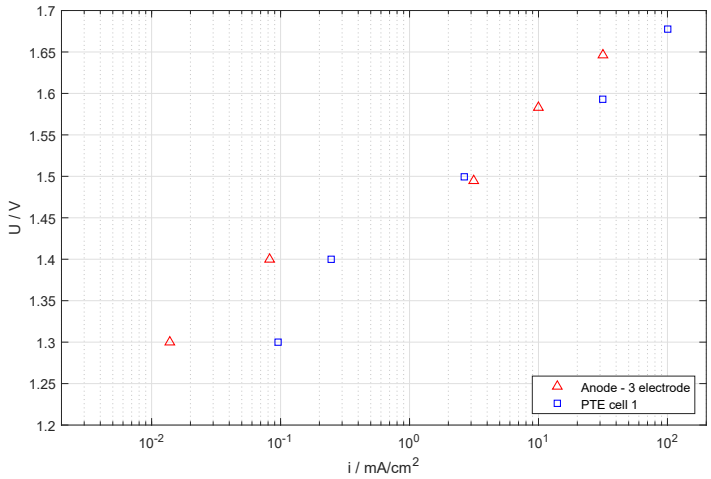

Fig. 11 – ALD high loading current densities from IR corrected CA: anode in three electrode setup (red) and PTE cell # 1 (blue). (For interpretation of the references to colour in this figure legend, the reader is referred to the Web version of this article.)

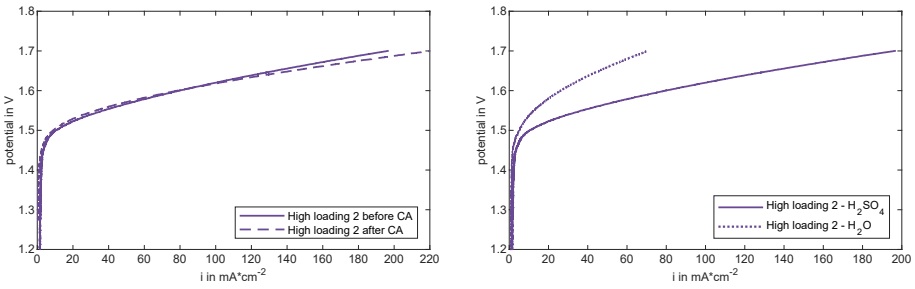

Fig. 12 – Polarization curves of the PTE cell # 2 (a) before and after the CA measurements and (b) operated with 1 mol/L sulphuric acid and deionised water.

As the oxygen evolution is the limiting electrolysis reaction we compare anode three electrode results with complete cell results using anodes with identical, high loadings. The Tafel plot in Fig. 11 displays U-i data points of the three electrode setup and the ALD high loading cell # 1. Voltages were consistently determined as described above in CA steps from 1.2 V to 1.7 V and IR corrected by using ASR_{EIS} values $1.7\Omega \cdot cm^2$ for 3 electrode), while current densities have been adjusted for leakage currents as described above. A sufficient qualitative agreement can be observed for cell voltages $\geq$1.4 V while the reported loss currents are dominating the complete cell data be1ow 1.4 V and are excluded.

Operating medium

PEM electrolysis cells are usually operated with water. Though the operation with 1 mol/l sulphuric acid would be feasible by repeatedly or continuously adding water to a sulphuric acid cycle, it can lead to significant corrosion. In this study, we observed a slight cell potential increase at low current densities after the CA measurements (see Fig. 12a) and a corrosion layer at the titanium end plates of the cell housing as a yellowish discolouration in the flow field area. However after the CA measurements the cell potential at higher current densities decreased and the leakage currents are reduced to 0.03 mA/cm^2. The decrease of the cell potential is attributed to an increased conductivity of the membrane and the reduced leakage currents indicate a subside of parasitic reactions. The comparable overpotential at low current densities indicate a rather stable exchange current densities and low corrosion effects.

For these reasons we additionally operated the cell with deionised water. The cell still achieves a current density of about 70 mA/cm^2 and thus 42% of the mean current density in sulphuric acid as can be seen in Fig. 12b. This current density is quite high if we take into account that the active area under water operation is likely to be reduced to the interface of the PTE fibres touching the membrane whereas the whole surface of the electrode is assumed to be active when operating with sulphuric acid. Further research is necessary and will be done to reach higher current densities under PTE cell operation with water.

Conclusion

In this study, we demonstrate the feasibility of a PEM electrolysis cell setup using porous transport electrodes with ALD catalyst coating. Several PTE cells were assembled and experimentally characterized. The setup turns out to be a promising candidate for catalyst loading reduction since the mean mass activity of 1400 A/g for $U = 1.7$ V clearly surpasses standard CCM cell values. Similar cell characteristics for three identical cells show the reproducibility of the PTE cell setup and assembly. The mean ASR is close to commercial cell values and exhibits a low variance. Increasing ALD loadings lead to increasing current densities for higher ALD as expected. The PTE cells in our study are operated in sulphuric acid in order to exclude PTE surface effects, but operation in water is shown to be feasible as well.

Though the mass activities are quite high compared to literature data, the mean current density 168 mA/cm^2 at $U = 1.7$ V is still low for a commercial application. The optimization of ALD coating for lowering the activation overpotentials is currently investigated. Due to the corrosive operating medium, a cell voltage limit of 1.7 V was set to prevent degradation of the cell components. By this way the process window and achievable current densities are strongly limited. Even though the change from CCM to PTE cell design is not affecting the porous structure, the coating potentially changes the gas transport and bubble release as observed by K. Dastafkan et al. [36] on Nickel foams. Gas transport and bubble release needs to be investigated. Further research efforts will investigate ionomer coatings of ALD PTEs for increasing the performance in water environment and the stability of coatings in sulphuric acid.

Declaration of competing interest

The authors declare that they have no known competing financial interests or personal relationships that could have appeared to influence the work reported in this paper.

Acknowledgements

This work was done within the research project Tubulyze and was supported by the German Federal Ministry of Education and Research (BMBF FKZ:03FS0564B).

The authors thank B. Sánchez Batalla and C.Weidlich (DECHEMA) for the ICP-MS measurements.

REFERENCES

[1] Bertuccioli L, Chan A, Hart D, Lehner F, Madden B, Standen E. Study on development of water electrolysis in the EU. Tech Rep Feb. 2014. E4tech, https://www.fch.europa.eu/sites/default/files/FCHJUElectrolysisStudy_FullReport%20(ID%20199214).pdf.

[2] Babic U, Suermann M, Büchi FN, Gubler L, Schmidt TJ. Critical review—identifying critical gaps for polymer electrolyte water electrolysis development. J Electrochem Soc 2017;164(4):F387–99. https://doi.org/10.1149/2.1441704jes.

[3] Bernt M, Siebel A, Gasteiger HA. Analysis of voltage losses in PEM water electrolyzers with low platinum group metal loadings. J Electrochem Soc 2018;165(5):F305–14. https://doi.org/10.1149/2.0641805jes.

[4] Hegge F, Lombeck F, Ortiz EC, Bohn L, von Holst M, Kroschel M, Hübner J, Breitwieser M, Strasser P, Vierrath S. Efficient and stable low iridium loaded anodes for PEM water electrolysis made possible by nanofiber interlayers. ACS Appl Energy Mater 2020;3(9):8276–84. https://doi.org/10.1021/acsaem.0c00735.

[5] Carmo M, Fritz DL, Mergel J, Stolten D. A comprehensive review on PEM water electrolysis. Int J Hydrogen Energy 2013;38(12):4901–34. https://doi.org/10.1016/j.ijhydene.2013.01.151.

[6] Kumar SS, Himabindu V. Hydrogen production by PEM water electrolysis – a review. Mater Sci Energy Technol 2019;2(3):442–54. https://doi.org/10.1016/j.mset.2019.03.002.

[7] Ayers K. The potential of proton exchange membrane–based electrolysis technology. Curr Opin Electrochem 2019;18:9–15. https://doi.org/10.1016/j.coelec.2019.08.008.

[8] Bernt M, Hartig-Weiß A, Tovini MF, El-Sayed HA, Schramm C, Schröter J, Gebauer C, Gasteiger HA. Current challenges in catalyst development for PEM water electrolyzers. Chem Ing Tech 2020;92(1–2):31–9. https://doi.org/10.1002/cite.201900101.

[9] Yu H, Danilovic N, Wang Y, Willis W, Poozhikunnath A, Bonville L, Capuano C, Ayers K, Maric R. Nano-size IrOx catalyst of high activity and stability in PEM water electrolyzer with ultra-low iridium loading. Appl Catal B Environ 2018;239:133–46. https://doi.org/10.1016/j.apcatb.2018.07.064.

[10] Ayers KE, Renner JN, Danilovic N, Wang JX, Zhang Y, Maric R, Yu H. Pathways to ultra-low platinum group metal catalyst loading in proton exchange membrane electrolyzers. Catal Today 2016;262:121–32. https://doi.org/10.1016/j.cattod.2015.10.019.

[11] Kúš P, Ostroverkh A, Ševčíková K, Khalakhan I, Fiala R, Skála T, Tsud N, Matolin V. Magnetron sputtered ir thin film on TiC-based support sublayer as low-loading anode catalyst for proton exchange membrane water electrolysis. Int J Hydrogen Energy 2016;41(34):15124–32. https://doi.org/10.1016/j.ijhydene.2016.06.248.

[12] Hrbek T, Kúš P, Yakovlev Y, Nováková J, Lobko Y, Khalakhan I, Matolín V, Matolínová I. Sputter-etching treatment of proton-exchange membranes: completely dry thin-film approach to low-loading catalyst-coated membranes for water electrolysis. Int J Hydrogen Energy 2020;45(41):20776–86. https://doi.org/10.1016/j.ijhydene.2020.05.245.

[13] Bühler M, Holzapfel P, McLaughlin D, Thiele S. From catalyst coated membranes to porous transport electrode based configurations in PEM water electrolyzers. J Electrochem Soc 2019;166(14):F1070–8. https://doi.org/10.1149/2.0581914jes.

[14] Bühler M, Hegge F, Holzapfel P, Bierling M, Suermann M, Vierrath S, Thiele S. Optimization of anodic porous transport electrodes for proton exchange membrane water electrolyzers. J Mater Chem 2019;7(47):26984–95. https://doi.org/10.1039/c9ta08396k.

[15] Fleming GJ, Fleming PJ. Development and optimization of porous carbon papers suitable for gas diffusion electrodes. Tech Rep Jan 2001. https://doi.org/10.2172/809960. final report, december 2000.

[16] Jiang X, Huang H, Prinz FB, Bent SF. Application of atomic layer deposition of platinum to solid oxide fuel cells. Chem Mater 2008;20(12):3897–905. https://doi.org/10.1021/cm7033189.

[17] Peng Q, Lewis JS, Hoertz PG, Glass JT, Parsons GN. Atomic layer deposition for electrochemical energy generation and storage systems. J Vac Sci Technol: Vac Surface Films 2012;30(1):010803. https://doi.org/10.1116/1.3672027.

[18] Bachmann J. Atomic layer deposition, a unique method for the preparation of energy conversion devices. Beilstein J Nanotechnol 2014;5:245–8. https://doi.org/10.3762/bjnano.5.26.

[19] Lee W-J, Bera S, Kim CM, Koh E-K, Hong W-P, Oh S-J, Cho E, Kwon S-H. Synthesis of highly dispersed pt nanoparticles into carbon supports by fluidized bed reactor atomic layer deposition to boost PEMFC performance. NPG Asia Mater jun 2020;12(1). https://doi.org/10.1038/s41427-020-0223-x.

[20] Musselman KP, Uzoma CF, Miller MS. Nanomanufacturing: high-throughput, cost-effective deposition of atomic scale thin films via atmospheric pressure spatial atomic layer deposition. Chem Mater 2016;28(23):8443–52. https://doi.org/10.1021/acs.chemmater.6b03077.

[21] Poodt P, Cameron DC, Dickey E, George SM, Kuznetsov V, Parsons GN, Roozeboom F, Sundaram G, Vermeer A. Spatial atomic layer deposition: a route towards further industrialization of atomic layer deposition. J Vac Sci Technol: Vac Surface Films 2012;30(1):010802. https://doi.org/10.1116/1.3670745.

[22] Schlicht S, Barr MKS, Wu M, Hoppe P, Spiecker E, Peukert W, Bachmann J. Minimization of catalyst loading on regenerative fuel cell positive electrodes based on titanium felts using atomic layer deposition. ChemElectroChem 2018;5(24):3932–7. https://doi.org/10.1002/celc.201801220.

[23] Schlicht S, Büttner P, Bachmann J. Highly active ir/TiO2 electrodes for the oxygen evolution reaction using atomic layer deposition on ordered porous substrates. ACS Appl Energy Mater 2019;2(3):2344–9. https://doi.org/10.1021/acsaem.9b00402.

[24] Schlicht S, Percin K, Kriescher S, Hofer A, Weidlich C, Wessling M, Bachmann J. Atomic layer deposition for efficient oxygen evolution reaction at pt/ir catalyst layers. Beilstein J Nanotechnol 2020;11:952–9. https://doi.org/10.3762/bjnano.11.79.

[25] Ressel S. Tubular all vanadium and vanadium/air redox flow cells. Ph.D. thesis. Universitat Politècnica de València; May 2019.

[26] Hofer A, Bochmann S, Bachmann J. Properties, performance and stability of iridium-coated water oxidation electrodes based on anodized titanium felts. Sustain Energy Fuel 2021;5(2):478–85. https://doi.org/10.1039/d0se01577f.

[27] Falcão D, Pinto A. A review on PEM electrolyzer modelling: guidelines for beginners. J Clean Prod 2020;261:121184. https://doi.org/10.1016/j.jclepro.2020.121184.

[28] Olivier P, Bourasseau C, Bouamama PB. Low-temperature electrolysis system modelling: a review. Renew Sustain Energy Rev 2017;78:280–300. https://doi.org/10.1016/j.rser.2017.03.099.
[29] Cooper K, Smith M. Electrical test methods for on-line fuel cell ohmic resistance measurement. J Power Sources 2006;160(2):1088–95. https://doi.org/10.1016/j.jpowsour.2006.02.086.
[30] Bender G, Carmo M, Smolinka T, Gago A, Danilovic N, Mueller M, Ganci F, Fallisch A, Lettenmeier P, Friedrich K, Ayers K, Pivovar B, Mergel J, Stolten D. Initial approaches in benchmarking and round robin testing for proton exchange membrane water electrolyzers. Int J Hydrogen Energy 2019;44(18):9174–87. https://doi.org/10.1016/j.ijhydene.2019.02.074.
[31] Immerz C, Paidar M, Papakonstantinou G, Bensmann B, Bystron T, Vidakovic-Koch T, Bouzek K, Sundmacher K, Hanke-Rauschenbach R. Effect of the MEA design on the performance of PEMWE single cells with different sizes. J Appl Electrochem 2018;48(6):701–11. https://doi.org/10.1007/s10800-018-1178-2.
[32] Kang Z, Alia SM, Young JL, Bender G. Effects of various parameters of different porous transport layers in proton exchange membrane water electrolysis. Electrochim Acta 2020;354:136641. https://doi.org/10.1016/j.electacta.2020.136641.
[33] Bromberger K, Ghinaiya J, Lickert T, Fallisch A, Smolinka T. Hydraulic ex situ through-plane characterization of porous transport layers in PEM water electrolysis cells. Int J Hydrogen Energy 2018;43(5):2556–69. https://doi.org/10.1016/j.ijhydene.2017.12.042.
[34] Parra-Restrepo J, Bligny R, Dillet J, Didierjean S, Stemmelen D, Moyne C, Degiovanni A, Maranzana G. Influence of the porous transport layer properties on the mass and charge transfer in a segmented PEM electrolyzer. Int J Hydrogen Energy 2020;45(15):8094–106. https://doi.org/10.1016/j.ijhydene.2020.01.100.
[35] Galbiati S, Morin A, Pauc N. Supportless platinum nanotubes array by atomic layer deposition as PEM fuel cell electrode. Electrochim Acta 2014;125:107–16. https://doi.org/10.1016/j.electacta.2014.01.061.
[36] Dastafkan K, Meyer Q, Chen X, Zhao C. Efficient oxygen evolution and gas bubble release achieved by a low gas bubble adhesive iron–nickel vanadate electrocatalyst. Small 2020;16(32):2002412. https://doi.org/10.1002/smll.202002412.